Journal of
Earth Science & Climatic Change

Raza et al., J Earth Sci Clim Change 2020, 11:2

Research Article Open Access

Stalagmite Based High Resolution $\delta^{18}O$ Record of Indian Summer Monsoon Activity in Lesser Himalaya during the late Holocene

Waseem Raza[1], Syed Masood Ahmad[2]*, Mahjoor Ahmad Lone[3], Drona Srinivasa Sarma[1], EVSSK Babu[1] and Chuan-Chou Shen[3]

[1]*CSIR-National Geophysical Research Institute, Hyderabad, India*
[2]*Department of Geography, Jamia Millia Islamia, New Delhi, India*
[3]*Department of Geosciences, National Taiwan University, Taipei 10617, Taiwan*

Abstract

The oxygen isotopic ($\delta^{18}O$) records from speleothems, particularly stalagmites, provide very valuable information to reconstruct paleomonsoon history. Here we present a high-resolution record of Indian summer monsoon (ISM) precipitation for the 2,851 and 677 year BP using a U-Th dated stalagmite sample from lesser Himalayan cave. The stalagmite (BGR1) may have been developed under the isotopic equilibrium condition as revealed by its almost identical $\delta^{18}O$ values of selected growth layers (Hendy test). X-ray diffraction analysis of BGR1 stalagmite shows predominance of calcite mineral. The $\delta^{18}O$ values exhibit significant changes (ranging from -6.92 to -10.24‰ *vs.* VPDB) during the studied time interval. Based on our $\delta^{18}O$ record, the climatic activity in lesser Himalaya can be categorized in two distinct phases, (a) a relatively dry period from 2,851 to 1,031 year BP and (b) a moderately wet period between 1,031 and 677 year BP. The spectral analysis of δ18O time series reveals a range of significant periodic components reflecting the control of solar activity on ISM variability.

Keywords: Oxygen isotope; Speleothem; Bageshwar cave; Paleomonsoon; Spectral analysis

Introduction

Monsoon systems are considered to be very complicated features of the earth's climate. Interestingly their intensities have varied significantly in the past as revealed by several marine and continental proxy records [1-8]. The Asian monsoon system (ASM) is the most widespread monsoon pattern in the world. The Indian summer monsoon (ISM) or southwest (SW) monsoon is one of the two leading monsoon patterns of Asian monsoon system. The climatic activity in Indian Himalayan region can be described by three different patterns i.e ISM, which is the main driver of climate and responsible for major rainfall over Indian subcontinent during June to September and July to August in the Western Himalayan region, Western Disturbances (WDs), a non-monsoonal precipitation driven by westerlies which carries winter rains in north and northwestern (NW) Indian regions during October to May and northeast (NE) monsoon also known as winter monsoon which brings rainfall in southern Indian region from October to December [9-13]. These patterns show the existence of diverse range of precipitation systems from east to west. The ISM penetrates from southwest direction to land and contributes about 80% precipitation of the total annual rainfall [14-16]. The rest of the precipitation will be received from NE monsoon and WDs (Westerlies).

The ISM variability since the LGM has been greatly dependent on marine sediment core records [17-23]. The other proxy records are mainly based on lacustrine sediments and lake-level studies, sediments from the Ganga plain and tree ring records from the western Himalaya [24-30]. The lacustrine sediments, which are usually considered to be the most commonly used archive of continental climate variability, generally have large chronological uncertainties and coarse resolution whereas marine proxies reflect incorporated effects of wind intensity, upwelling and river discharge not precipitation changes directly [31,32]. This limitation with lacustrine and marine sediments has inclined the researchers to make use of speleothems specially stalagmites as a best suitable archive for continental paleoclimate information because it provides a direct record of changes in the ISM rainfall assuming that temperature variations are very small in the tropical region on millennial time scale. The advantage of using speleothems is its precise chronological character by U-Th dating technique and recent advancement in modelling techniques of U-Th derived ages.

The Himalayan region has experienced a number of wet and dry periods since the beginning of Holocene [33]. Several studies reveal the weakening in monsoon intensity during the various cold events [34,35]. The precipitation variability at different locations of Indian subcontinent and elsewhere, primarily influenced by ISM, has been reconstructed by several workers using well dated stalagmites [36-44]. It is also recognized that the Westerlies influences climatic activity in the Himalayan region in addition to the ISM. High-resolution climatic events from the Central Himalayan region, particularly during the mid and late Holocene are either less implicit or scattered. Also there is a scarcity of precipitation records from precisely of dated speleothems between Pleistocene and Holocene transition [34]. An attempt is made here to infer late Holocene precipitation changes in lesser Himalaya through oxygen isotopes of a calcitic stalagmite.

Geological Setting, Climate and Location of the Cave

The Bageshwar cave (29° 49′ N: 79° 46′ E) is located near Garikhet village of Bageshwar district, Uttrakhand in the lesser Himalayan region and lies roughly about 50 feet above the road with an elevation of around 1,004 m above mean sea level (Figure 1). A 16 cm long stalagmite was collected in the month of April, 2015. The cave is around 11 m long with main entrance of 1.5 m x 1 m and becomes narrow as approaches towards the end of the cave. The sample was collected at the distance of 7 m from the entrance. The stalagmite sample was

***Corresponding author:** Syed Masood Ahmad, Department of Geography, Jamia Millia Islamia, New Delhi, India; E-mail: smasoodahmad@rediffmail.com

Received October 30, 2019; **Accepted** January 23, 2020; **Published** February 01, 2020

Citation: Raza W, Ahmad SM, Lone MA, Sarma DS, Babu EVSSK, et al. (2020) Stalagmite Based High Resolution $\delta^{18}O$ Record of Indian Summer Monsoon Activity in Lesser Himalaya during the late Holocene. J Earth Sci Clim Change 11: 527

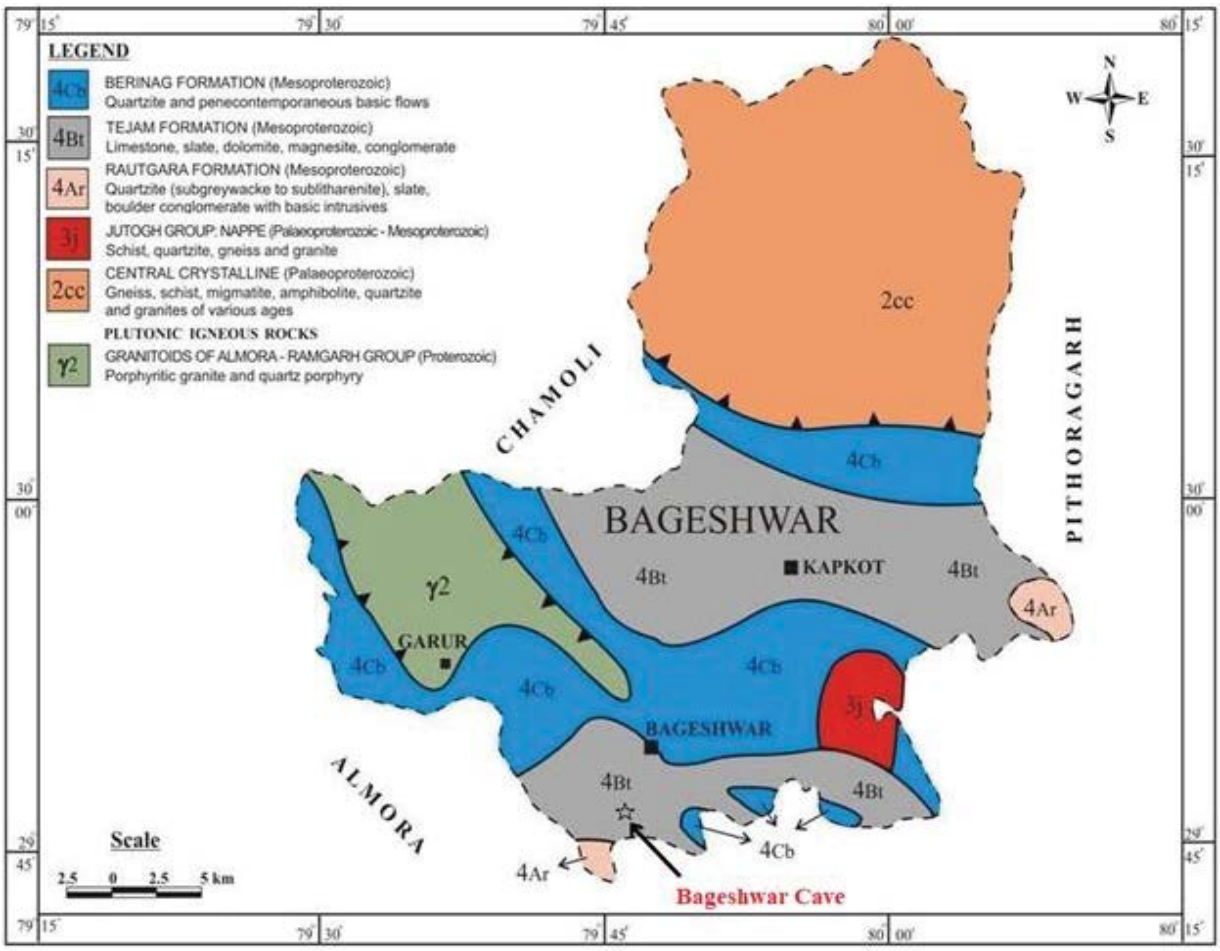

Figure 1: Geological map of the area around Bageshwar Cave, Uttarakhand (modified after CGWB, India).

formed from overlying Mesoproterozoic limestone formation, about 50 m above the cave. The climate of the region is temperate to sub-humid with warm/wet summer and cool/dry winter. The mean annual precipitation is about 1220 mm with average high (330 mm) and low (6 mm) precipitation occurs in July and November respectively and 80% of the precipitation falls during the monsoon months from June to September (Figure 2a). The mean annual $\delta^{18}O_{VSMOW}$ of precipitation with 95% CI (0.4‰) is around −8.10‰ [45] (Figure 2a). The humidity and temperature inside the cave was recorded as 77% and 27°C respectively at the time of sampling. The humidity in nearby region will be as low as 30% in the pre-monsoon period and increases rapidly with the onset of monsoon and attains at about 80% during July to September whereas the mean maximum and minimum temperatures are reported as 25°C and 15°C respectively (Data from Central Ground Water Board, India). The sample is composed of calcite with clearly visible growth layers and does not show any indication of discontinuity or depositional disruption (Figure 2b). The surrounding vegetation is dominated by Chir Pine, Himalayan Cypress and small shrubs.

Materials and Methods

A 16 cm long stalagmite sample (BGR1) was collected from the Bageshwar cave located in Uttarakhand state of India during July 2015. The extracted stalagmite was cut along its growth axis using a diamond cutter to make slices for sub-sampling. The sliced portions of the sample was polished and cleaned systematically using distilled water pursued by ultrasonic bath followed by drying at room temperature. Micro-drilling of the sliced sample was then performed at CSIR-National Geophysical Research Institute, Hyderabad using a micro-drilling machine (MANIX-180) with a drill bit of 0.8 mm to acquire powdered samples for isotopic and mineralogical analysis.

Hendy test was performed on selected on samples from growth layers of BRG1 to ensure that the stalagmite was deposited under isotopic equilibrium with precipitating water [46]. Five sub-samples from three different growth layers were taken for oxygen and carbon isotopic measurements on MAT-253 model of IRMS (Isotope Ratio Mass Spectrometer) coupled with an automated Kiel-IV carbonate device at CSIR-NGRI, Hyderabad, India. The X-ray Diffraction (XRD) technique was used to further establish the mineralogical composition of the stalagmite sample. Four sub-samples (1 gm each) were drilled from different portions (top to bottom) of the sample using micro-drilling machine (MANIX-180) with a drill bit of 1 mm for XRD. The XRD analysis of the sample was performed on a Philips X-ray diffractometer using nickel filtered Cu Kα radiation at the CSIR- NIO, Goa [47]. The $^{230}Th/U$ dating technique was used to determine ages of BGR1 stalagmite. Four different layers were selected for U-Th dating using a Thermo Fisher NEPTUNE multi-collector inductively couples plasma mass spectrometer (MC-ICP-MS) at the High-Precision Mass Spectrometry and Environment Change Laboratory (HISPEC) at

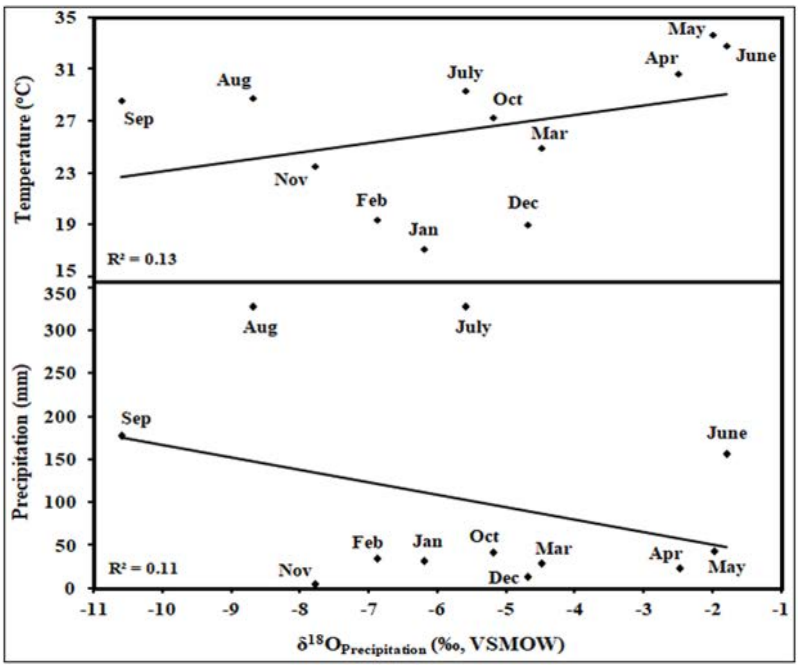

Figure 2: Graph showing mean monthly temperature and $\delta^{18}O$ of Precipitation (Source: www.imd.gov.in) at Bageshwar, indicating that the precipitation during the monsoon season generally has lower $\delta^{18}O$.

National Taiwan University, Taiwan following the method developed by Shen [48]. Details of instrumental procedure including off-line data reduction were described in Shen [49]. All the dates (year BP) are in correct stratigraphic order with a 2 sigma error ranging from ± 89 to ± 934 yrs. It may be noted that except one age point all other three ages obtained show errors within ± 149 yrs. The StalAge program was used to construct the age-depth model of BGR1 stalagmite and to minimize age uncertainties. This StalAge program is mainly based on an algorithm developed by Scholz and Hoffmann [50]. This algorithm utilizes ^{230}Th ages with their associated age uncertainty and also incorporates the stratigraphic information to improve the age model and provides the results (ages) with 95% confidence level using a Monte-Carlo simulation.

Powdered drilled subsamples were reacted with saturated orthophosphoric acid (100% H_3PO_4) at 70 °C in a vacuum system and the evolved CO_2 was analyzed for $\delta^{18}O$ measurements by Isotope Ratio Mass Spectrometer (IRMS) [51,52]. The δ 18O measurements were carried out at the CSIR-National Geophysical Research Institute, Hyderabad, using a MAT-253 model of IRMS attached with a Kiel-IV automated carbonate device. To ensure reproducibility of the instruments, international carbonate standards (NBS-18 and NBS-19) were analyzed with every batch of 8 samples. The calibration to the VPDB standard was achieved by repeated measurements of international reference standards NBS-18 and NBS-19 [53]. Isotopic results are expressed against Vienna Pee Dee Belemnite (VPDB) standard and analytical precision was found to be better than ± 0.06‰ for δ 18O. The δ 18O record of BGR1 was used to explore periodic components of time series by using spectral analysis. The common nature of paleoclimate time series is its unevenness (unevenly spaced) and our δ 18O time series is also unequally spaced in time. Ólafsdóttir has demonstrated that the data interval and its resolution are important properties of any climate time series [54]. The spectral analysis of BGR1 $\delta^{18}O$ time series was carried out using REDFIT procedure of Schulz and Mudelsee in PAleontological STatistics (PAST) v. 3.4 software [55]. This REDFIT program is based on Lomb-Scargle Fourier transform and has been specifically developed to address unevenly spaced paleoclimate time series [56-58].

Results and Discussion

Hendy has proposed that $\delta^{18}O$ values should be almost identical within a single growth layer to ensure absence of any kinetic fractionation during the deposition of the stalagmite [46]. We have performed Hendy test in sub-samples taken from three distinct layers by analyzing both $\delta^{18}O$ and $\delta^{13}C$ from depths of 2.9; 7.3 and 14.0 cm of BGR1 sample. The results of Hendy test indicate that, neither there is a significant variation in $\delta^{18}O$ nor a correlation between $\delta^{18}O$ and $\delta^{13}C$ along the same growth layer, and hence the stalagmite might have been formed under isotopic equilibrium conditions (Figure 3). Some researchers have argued that speleothems can still be utilized as a proxy for precipitation despite the failure of Hendy test, because $\delta^{18}O$ values of a speleothem calcite controlled mainly by precipitation changes rather than the temperature and thus it is not obligatory for the stalagmites to grow under isotopic equilibrium with cave drip water to provide information about the past climatic conditions [59-65]. Zhou provided evidence that stalagmite $\delta^{18}O$ values can be considered as a dependable precipitation proxy if subsamples for isotopic measurements are taken from the central growth axis [66].

The U-Th dates of four subsamples of BGR1 are displayed in Table 1 and their plot with respect to sample depths in Figure 4. All the ages were found to be in chronological order with values ranging from 2,342 to 919 year BP and the age uncertainties ranging from ± 89 to ± 934 years (2 σ). The diverse range of growth rate for different segments of BGR1 stalagmite reveals nonlinear nature of its development and hence linear interpolation may not be an ideal method for precise age determination. Therefore we adopted StalAge model (age-depth), which is based on Monte-Carlo simulation to deduce ages for each δ

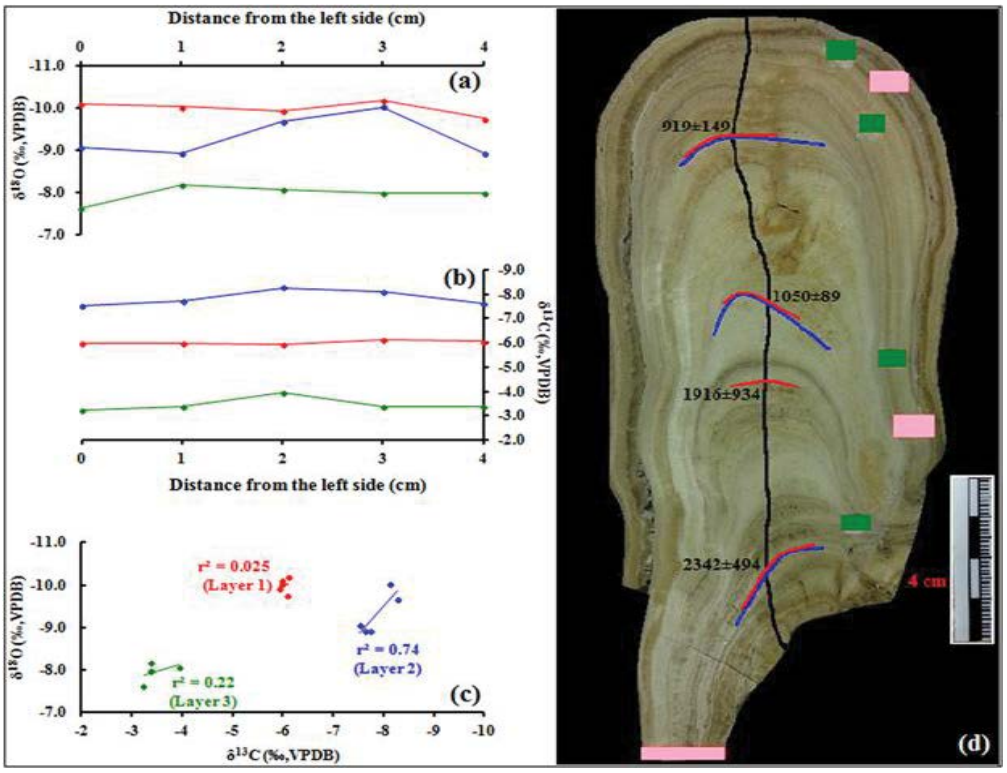

Figure 3: Hendy test results. Red, blue and green lines represent three dissimilar test layers. (a) δ^{18}O values (b) δ^{13}C values (c) Shows correlation between δ^{18}O and δ13C R^2 in represents that the sample formed under equilibrium conditions (d) BGR1 stalagmite- Black line represents the drilling points for δ^{18}O measurements. Red lines represent four ^{230}Th dating samples. Blue lines show layers of Hendy test. Green boxes represent four XRD analysis points.

sample ID	Weight (g)	^{230}UPP^{ba}	^{232}Thpp^{t}	d^{234}U Measured^{a}	[^{230}Th/^{238}U] activity^{c}	[^{230}Th/^{232}Th] ppm^{d}	Age (yr BP) Uncorrected	Age (yr BP) corrected^{c,d}	Age (yr BP) relative to 1950 AD	d^{234}Uinitial corrected^{b}
V6	0.0759	682.61 ± 0.88	7582 ± 21	5.9 ± 1.7	0.01174 ± 0.00024	17.43 ± 0.36	1280 ± 27	988 ± 149	919 ± 149	5.9 ± 1.7
V7	0.086	950.2 ± 1.4	6207 ± 16	2.7 ± 1.6	0.01180 ± 0.00020	29.79 ± 0.51	1291 ± 22	1119 ± 89	1050 ± 89	2.7 ± 1.6
V8	0.0683	999.8 ± 1.2	68572 ± 521	0.0 ± 1.3	0.0344 ± 0.0013	8.26 ± 0.32	3814 ± 149	1984 ± 934	1916 ± 934	0.0 ± 1.3
V9	0.0707	1219.6 ± 1.5	44149 ± 257	-1.0 ± 1.4	0.03044 ± 0.00092	13.86 ± 0.43	3374 ± 104	2411 ± 494	2342 ± 494	-1.0 ± 1.4

Table 1: Uranium and Thorium Isotopic compositions and 230Th ages for BGR1 sample by MC-ICPMS, Thermo Electron Neptune at NTU.

18O value [50]. However a linear model was also constructed for all δ 18O values to compare it with the StalAge model. The linear age model constructed for BGR1 shows a reasonable good agreement with StalAge model (Figure 5).

Mineralogical composition of the BGR1 stalagmite, established by XRD analysis confirms predominance of calcite mineral with low Mg content (Figure 6). The surface of the sample shows apparent and continuous layering without any critical lithological alteration. The δ 18O values range from -6.92 to -10.24‰ *vs.* VPDB with an average value of -8.29‰. The variation of 3.32‰ in δ^{18}O is relatively higher than the Peninsular Indian stalagmites [67]. Other studies from Himalayan stalagmites have also reported higher variations in δ 18O compared to Peninsular stalagmites [13,34,68,69]. It is rational to take mean δ 18O of -8.29‰ as a reference value representing the average climatic conditions for the time interval of the BGR1 stalagmite precipitation. The δ 18O variations in BGR1 stalagmite clearly demonstrates the two distinct phases of climatic activity (Figure 7). These phases can be described as, (i) a phase from 2,851 to 1,031 yr BP, of fluctuating δ 18O values ranging from -9.75 to -6.92‰, with an average δ 18O value of -8.06‰, dominated by relatively enriched δ 18O values representing shifts in precipitation during this period, and (ii) another phase between 1,031 and 677 yr BP, represented by depleted δ 18O values from -10.24 to -7.75‰ with an average δ 18O of -8.73‰. The average δ 18O value of -8.06‰ from 2,851 to 1,031 yr BP is higher than the average δ 18O value (-8.29‰) indicating relatively dry and arid conditions during this period, with lowest precipitation occurring at around 2,173 yr BP (characterized by most enriched δ 18O of -6.92‰). This arid period was punctuated by three wet events at around 2717, 2333 and 1732 yr BP, with highest precipitation occurred at around 2,717 yr BP, reflected by most depleted δ 18O value of -9.75‰. Further, this dry period was followed by a moderately wet period between 1,031 and 677 yr BP as reflected by average δ 18O value of -8.73‰, lesser than the average δ 18O value (-8.29‰) of BGR1 stalagmite with highest precipitation occurring around 797 yr BP manifested by most depleted δ 18O value of -10.24‰. This wet period between 1,031 and 677 yr BP was interrupted by three dry events at approximately 914, 809 and 687

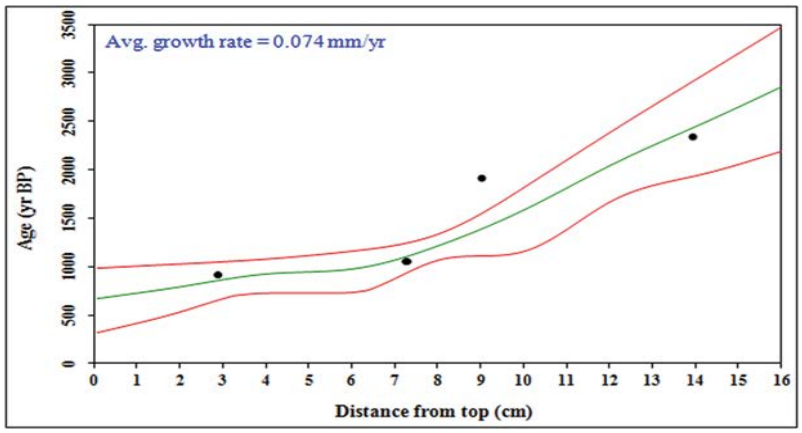

Figure 4: The StalAge model of BGR1. Green line represents modeled ages and red lines show 95% confidence limits. The black dots represent four ^{230}Th samples. The average growth rate as shown is 0.07 mm/yr.

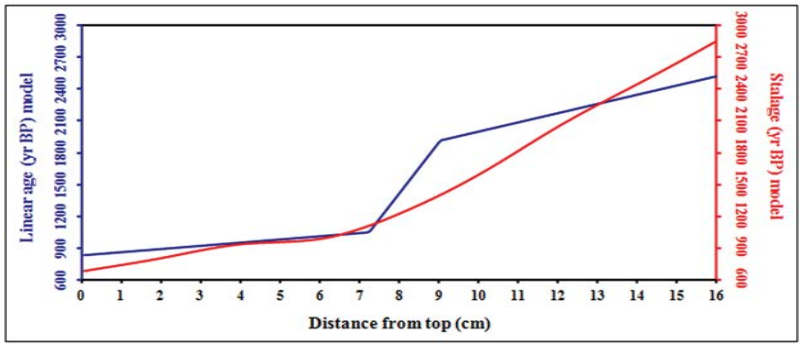

Figure 5: Comparing linear and StalAge models.

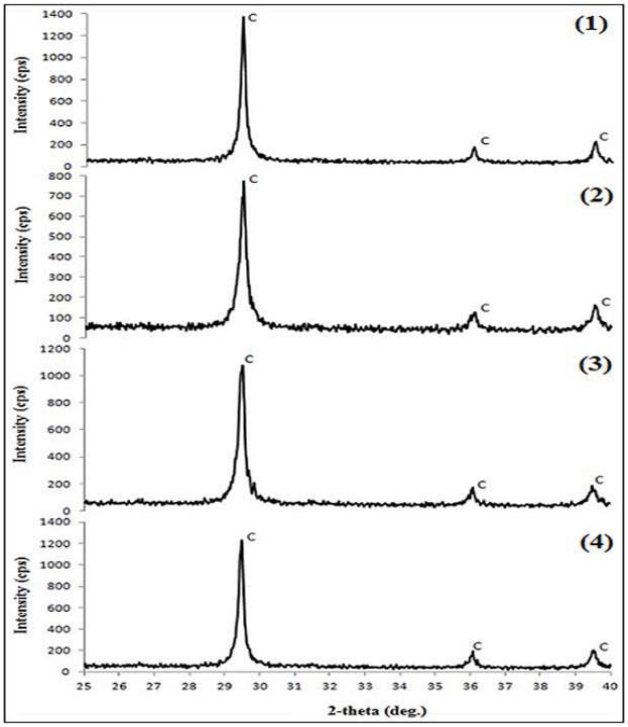

Figure 6: Graph showing mineralogical composition of BGR1 stalagmite from four different depths by X-ray diffraction analysis revealing predominance of calcite mineral. The x-axis shows the diffraction angle (˚C) and y-axis shows the intensity (counts per second) as a function of diffraction angle.

yr BP, with lowest precipitation occurred at around 809 yr BP, marked by most enriched δ 18O value of -7.75‰.

The ISM has a very strong influence on δ^{18}O of speleothems from Chinese caves [70]. The comparison of our BGR1 stalagmite record with stalagmites from China have also demonstrated influence of ISM in central China and Tan reflects coincident variations in precipitation strength during the late Holocene [71-73] (Figure 8). Wang and Chen demonstrate that atmospheric water vapor over southern China is mainly carried from the Indian Ocean [74]. The Figure 8 shows that the analogous tendency of δ 18O values in BGR1 and Chinese speleothems during the late Holocene confirm synchronous variability in Asian monsoon systems (Figure 8).

Spectral analysis of BGR1 δ 18O time series reveals a range of significant periodicities (Figure 9). The average resolution of entire δ^{18}O time series is ~9 years. Two peaks at around 0.026 and 0.03 cycles per year (~38 and 33 years cycle) were observed with 99% and 90% significance level respectively (Figure 9). A cycle of 33-38 years was reported by Stocker (1994) has been recognized as natural fluctuations of thermohaline circulation in North Atlantic. A solar cycle of 32 year has been reported by Tiwari from a tree ring record from the western Himalaya. In addition, a 33 years cycle has been reported from speleothem records from China and a 36 year cycle was reported by Cai [75-80]. In view of available literature, this 33 years cycle in BGR1 attribute to solar forcing control on ISM dynamics. The long term cycle of ~436 years is almost similar to the 420 years cycle observed in VSPM1 δ^{18}O time series [52] (Figure 9). Stuiver and Braziunas detected this 420 years cycle by investigating high precision 14C chronology and related this cycle to periodic variations in the solar constant. Hence, these cycles may be reflecting the control of solar activity on ISM variability [81].

Conclusion

The 2,200 year δ^{18}O time series from a stalagmite sample collected from the lesser Himalaya exhibit high amplitude variations in ISM precipitation during the late Holocene. The data reveals changes in ISM activity on multi-decadal to centennial timescales during the late Holocene. The δ^{18}O time series provides a strong signature of significant changes in ISM activity between 2,851 and 677 yr BP. The δ^{18}O record shows a relatively dry period from 2,851 to 1,031 yr BP in lesser Himalaya, followed by wet conditions between 1,031 and 677 yr BP. A prominent δ^{18}O shift, indicating enhance ISM activity at ~ 1000 yr BP is also reflected in sudden increase in growth rate of BGR1 stalagmite. Spectral analysis of BGR1 δ^{18}O time series suggests 436, 38, 33-year cycles indicating mainly solar control on ISM dynamics for the studied time interval. A comparison of BGR1 δ^{18}O time series with those of Chinese stalagmites shows synchronous variations in monsoon-induced precipitation during the late Holocene.

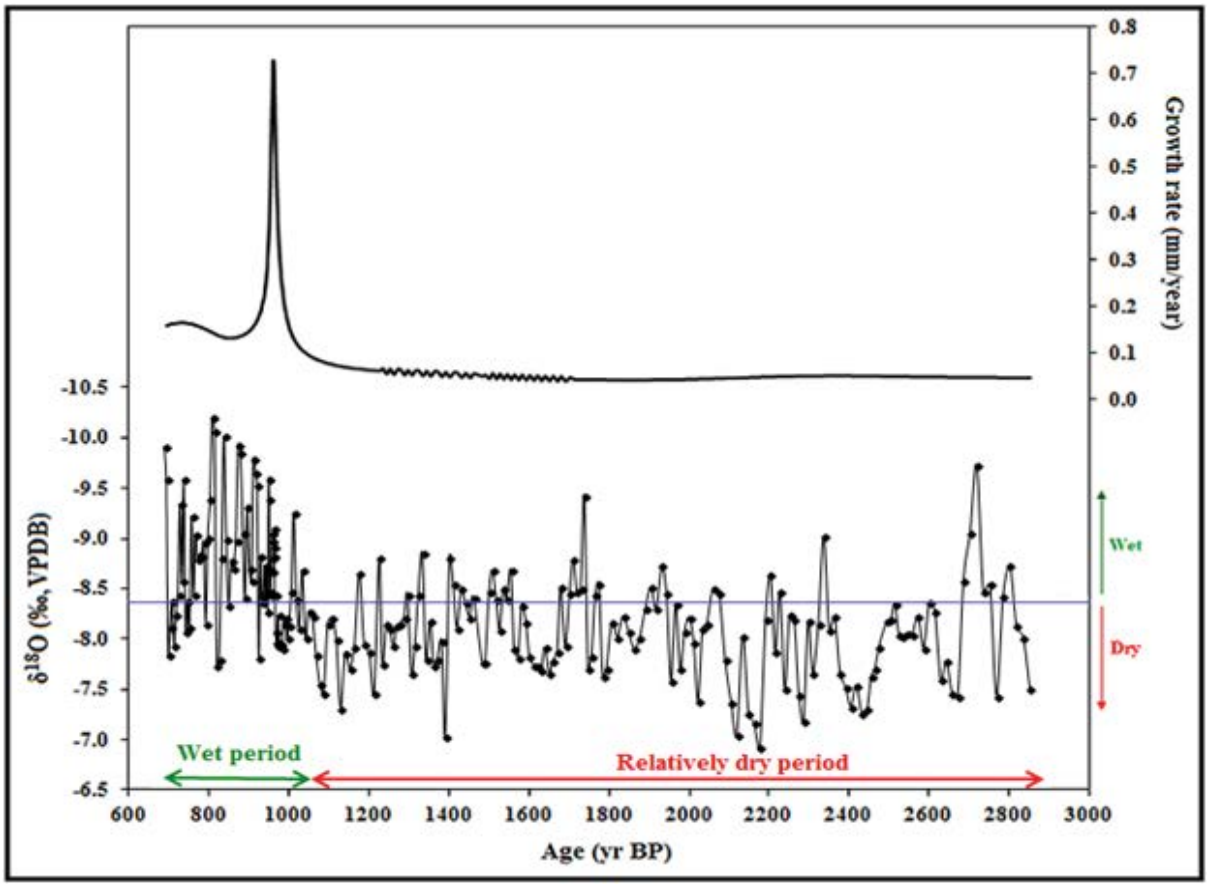

Figure 7: Graph showing variations in δ^{18}O *vs* VPDB with growth rate of the BGR1 stalagmite between 2,851 and 677 yr BP. Blue line represents average δ^{18}O of BGR1 stalagmite. Relatively dry period from 2,851 to 1,031 yr BP is indicated by red line followed by a wet period between 1,031 and 677 yr BP, shown by green line.

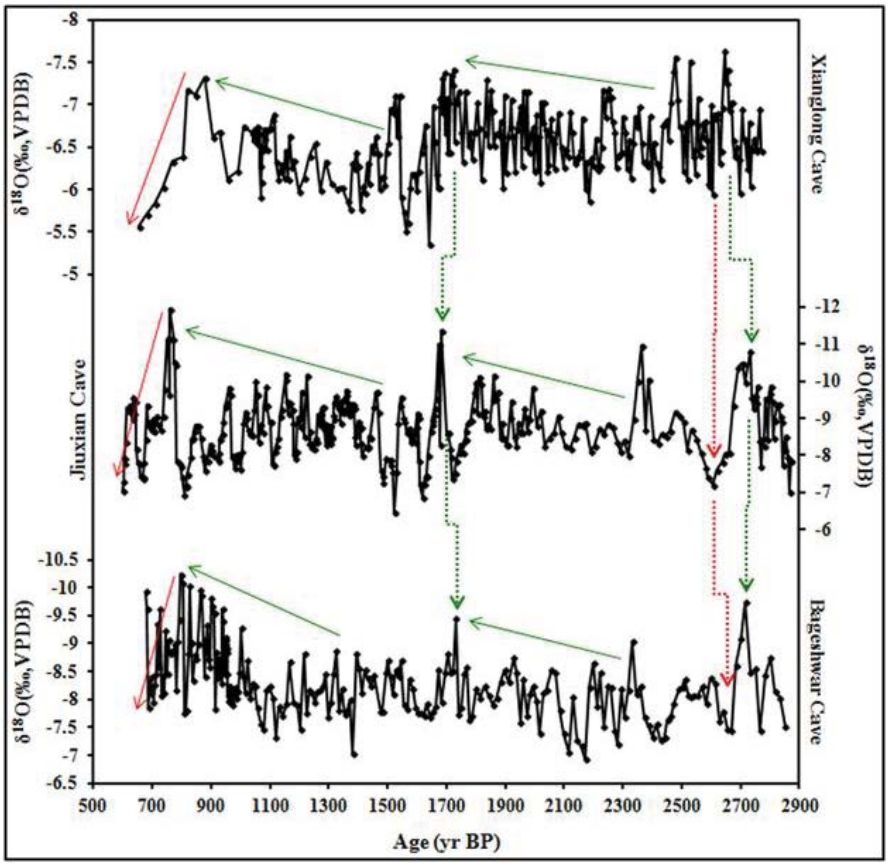

Figure 8: Comparison between the δ^{18}O time series of BGR1 with Chinese cave records. The vertical green and red dotted lines represent the coincident highest and lowest precipitation events respectively, whereas the green and red lines correspond to periods of strengthen and weaken monsoon activity respectively within their age uncertainties.

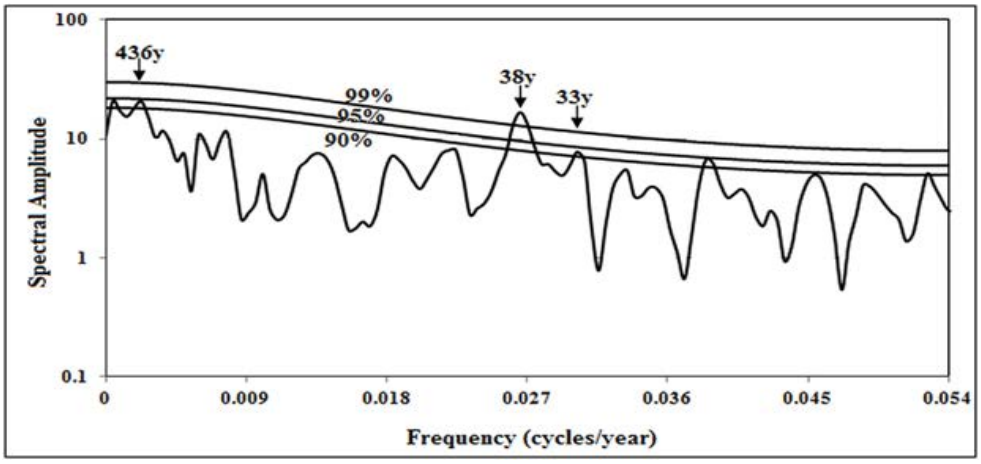

Figure 9: Spectral analysis of BGR1 δ^{18}O time series using REDFIT 3.8 program. Peaks indicated by arrows are representing the 436, 38 and 33 year cycles.

Acknowledgements

The authors are thankful to Dr. V. M. Tiwari, Director, CSIR-NGRI, Hyderabad. The first author is thankful to Ms. K. Zainab and colleagues at Geochronology & Isotope Studies group, CSIR-NGRI for their support. We are also grateful to the Council of Scientific and Industrial Research (CSIR) for analytical support provided during this study. We are also thankful to the National Taiwan University for providing the U-Th dates of BGR1 sample.

References

1. McClure HA (1976) Radiocarbon chronology of late Quaternary lakes in the Arabian Peninsula. Nature 263: 755-756.
2. Gasse F, Street FA (1978) Late Quaternary lake-level fluctuations and environments of the northern Rift Valley and Afar region (Ethiopia and Djibouti): Palaeogeogr Palaeocl 24: 279-325.

3. Bryson RA, Swain AM (1981) Holocene variations of monsoon rainfall in Rajasthan: Quaternary Res 16: 135-145.

4. Ritchie JC, Eyles CH, Haynes CV (1985) Sediment and pollen evidence for an early to mid-Holocene humid period in the eastern Sahara. Nature 314:352-355.

5. Clemens SC, Prell WL, Murray D, Shimmield G, Weedon G (1991) Forcing mechanisms of the Indian Ocean monsoon. Nature 353: 720-725.

6. Sirocko F, Sarnthein M, Erlenkeuser H, Lange H, Arnold M, et al. (1993) Century-scale events in monsoonal climate over the last 24 000 years. Nature 364: 322-324.

7. Overpeck J, Anderson D, Trumbore S, Prell W (1996) The southwest Indian monsoon over the last 18 000 years: Clim Dynam 12: 213-225.

8. Burns SJ, Matter A, Frank N, Mangini A (1998) Speleothem-based paleoclimate record from northern Oman. Geology 26: 499-502.

9. Chalise SR, Khanal NR (2001) An introduction to climate, hydrology and landslide hazards in the hindu kush-himalayan region In Landslide Hazard Mitigation in the Hindu Kush-Himalayas. 63-70.

10. Kotlia BS, Ahmad SM, Zhao Jian-Xin, Raza W, Collerson KD (2012) Climatic fluctuations during the LIA and post-LIA in the Kumaun Lesser Himalaya, India: Evidence from a 400 yr old stalagmite record. Quatern Int 263: 129-168.

11. Kotlia BS, Singh AK, Zhao JX, Duan W, Tan M, et al. (2017) Stalagmite based high resolution precipitation variability for past four centuries in the Indian Central Himalaya: Chulerasim cave re-visited and data re-interpretation. Quatern Int 444: 34-35.

12. Liang F, Brook GA, Kotlia BS, Railsback LB, Hardt B, et al. (2015) Panigarh cave stalagmite evidence of climate change in the Indian Central Himalaya since AD 1256: Monsoon breaks and winter southern jet depressions. Quaternary Sci Rev 124: 145-161.

13. Joshi LM, Kotlia BS, Ahmad SM, Wu CC, Sanwal J, et al. (2017) Reconstruction of Indian monsoon precipitation variability between 4.0 and 1.6 ka BP using speleothem $\delta^{18}O$ records from the Central Lesser Himalaya, India. Arab J Geosci 10:pp: 356.

14. Rao YP (1976) Southwest Monsoon. Meteorological Monograph, India Meteorological Department, New Delhi. 1: pp: 366

15. Agnihotri R, Dutta K, Bhushan R, Somayajulu BLK (2002) Evidence for solar forcing on the Indian monsoon during the last millennium. Earth Planet Sc Lett 198: 521-527.

16. Gadgil S (2003) The Indian Monsoon and its variability. Annual Review of Earth Planet Sc Lett 31: 429-467.

17. Sirocko F, Grabe Schonberg D, Mcintyre A, Molfino B (1996) Teleconnection between subtropical monsoon and highlatitude climates during the last glaciation. Science 272: 526-529.

18. Zonneveld KAF, Ganssen G, Troelstra S, Versteegh GJM, Visscher H (1997) Mechanisms of forcing abrupt fluctuations of the Indian Ocean summer monsoon during the last deglaciation. Quaternary Sci Rev 16: 187-201.

19. Schulz H, Von Rad U, Erlenkeuse H (1998) Correlation between Arabian Sea and Greenland climate oscillations of the past 11,000 years. Nature, 393: 54-57.

20. Von Rad U, Schaaf M, Michels KH, Schulz H, Berger WH, et al. (1999) A 5000 year record of climate change in varved sediments from the oxygen minimum zone off Pakistan, Northeastern Arabian Sea. Quaternary Res 51:39-53.

21. Anderson DM, Overpeck JT, Gupta AK (2002) Increase in the Asian southwest monsoon during the past four centuries. Science, 297: 596-599.

22. Gupta A, Anderson DM, Overpeck JT (2003) Abrupt changes in the Asian southwest monsoon during the Holocene and their links to the North Atlantic Ocean. Nature 421: 354-357.

23. Jung SJA, Davies GR, Ganssen GM, Kroon D (2004) Synchronous Holocene sea surface temperature and rainfall variations in the Asian monsoon system. Quaternary Sci Rev 23: 2207-2218.

24. Enzel Y, Ely LL, Mishra S, Ramesh R, Amit R, et al. (1999) High-resolution Holocene environmental changes in the Thar Desert, Northwestern India. Science 284: 125-128.

25. Sharma S, Joachimski M, Tobschall H, Singh H, Sharma C, et al. (2004) Late glacial and Holocene environmental changes in Ganga plain, northern India. Quaternary Sci Rev 23: 145–159.

26. Sharma S, Joachimski MM, Tobschall HJ, Singh IB, Sharma C, et al. (2006) Correlative evidences of monsoon variability, vegetation change and human inhabitation in Sanai lake deposit: Ganga Plain, India. Curr Sci India 90: 973-978.

27. Agrawal S, Sanyal P, Sarkar A, Jaiswal MK, Dutta K (2012) Variability of Indian monsoonal rainfall over the past 100 ka and its implication for C3-C4 vegetational change. Quaternary Res 77: 159-170.

28. Yadav R, Singh J (2002) Tree-ring-based spring temperature patterns over the past four centuries in western Himalaya. Quaternary Res 57: 299-305.

29. Phadtare N, R Pant (2006) A century-scale pollen record of vegetation and climate history during the past 3500 years in the Pinder Valley, Kumaon Higher Himalaya. J Geol Soc India 68: 495-506.

30. Sano M, Ramesh R, Sheshshayee MS, Sukumar R (2011) Increasing aridity over the past 223 years in the Nepal Himalaya inferred from a tree ring 18O chronology. Holocene 22: 809-817.

31. Burns SJ, Fleitmann D, Matter A, Neff U, Mangini A (2001) Speleothem evidence from Oman for continental pluvial events during interglacial periods. Geology 29: 623-626.

32. Laskar AH, Yadava MG, Ramesh R, Polyak VJ, Asmerom Y (2013) A 4 kyr stalagmite oxygen isotopic record of the past Indian Summer Monsoon in the Andaman Islands. Geochem Geophy Geosy 14: 3555-3566

33. Phadtare NR (2000) Sharp decrease in summer monsoon strength 4000-3500 cal yr BP in the Central Higher Himalaya of India based on pollen evidence from alpine peat. Quaternary Res 53: 122-129.

34. Sinha A, Cannariato KG, Stott LD, Li HC, You CF (2005) Variability of Southwest Indian summer monsoon precipitation during the Bolling-Allerod. Geology 33: 813-816.

35. Kotlia BS, Sanwal J, Phartiyal B, Joshi LM, Trivedi A, et al. (2010) Late Quaternary climatic changes in the eastern Kumaun Himalaya, India, as deduced from multi-proxy studies. Quatern Int 213: 44-55.

36. Yadava MG, Ramesh R, Pant GB (2004) Past monsoon rainfall variations in peninsular India recorded in a 331-year-old speleothem. Holocene 14: 517-524.

37. Yadava MG, Ramesh R (2005) Monsoon reconstruction from radiocarbon dated tropical Indian speleothems. Holocene 15: 48-59.

38. Yadava MG, Ramesh R (2006) Stable oxygen and carbon isotope variations as monsoon proxies: a comparative study of speleothems from four different locations in India. J Geol Soc India 68: 461-475.

39. Fleitmann D, Burns SJ, Mangini A, Mudelsee M, Kramers J (2007) Holocene ITCZ and Indian monsoon dynamics recorded in stalagmites from Oman and Yemen (Socotra). Quaternary Sci Rev 26: 170-188.

40. Shakun JD, Burns SJ, Fleitmann D, Kramers J, Matter A (2007) A high resolution, absolute-dated deglacial speleothem record of Indian Ocean climate from Socotra Island. 259: 442-456.

41. Sinha A, Cannariato KG, Stott LD, Cheng H, Edwards RL (2007) A 900 year (600 to 1500 AD) record of the Indian summer monsoon precipitation from the core monsoon zone of India. Geophys Res Lett 34: 16

42. Sinha A, Berkelhammer M, Stott L, Mudelsee M, Cheng H (2011a) The leading mode of Indian Summer Monsoon precipitation variability during the last millennium. Geophys Res Lett 38: 15

43. Sinha A, Stott L, Berkelhammer M, Cheng H, Edwards RL (2011b) A global context for megadroughts in monsoon Asia during the past millennium. Quaternary Sci Rev 30: 47-62.

44. Kaushal N, Sebastian F, Breitenbach M, Lechleitner FA, Sinha A, et al. (2018) The Indian Summer Monsoon from a Speleothem Perspective: A Review. Quaternary 1: 29.

45. Bowen GJ, Revenaugh J (2003) Interpolating the isotopic composition of modern meteoric precipitation. Water Resour Res 39: 1299.

46. Hendy CH (1971) The isotopic geochemistry of speleothems-I. The calculation of the different modes of formation on the isotopic composition of speleothems and their applicability as paleoclimatic indicators. Geochim Cosmochim Ac 35: 801-824.

47. Kessarkar PM, Rao VP, Shynu R, Mehra P, Viegas BE (2010) The nature and distribution of particulate matter in the Mandovi Estuary, central west coast of India. Estuaries Coasts 33: 30-44.

48. Shen CC, Wu CC, Cheng H, Edwards RL, Hsieh YT, et al. (2012) High-precision and high-resolution carbonate ^{230}Th dating by MC-ICP-MSwith SEM protocols. Geochim Cosmochim Ac 99: 71-86.

49. Shen CC, Edwards RL, Cheng H, Dorale JA, Thomas RB, et al. (2002) Uranium and thorium isotopic and concentration measurements by magnetic sector inductively coupled plasma mass spectrometry. Chem Geol 185: 165-178.

50. Scholz D, Hoffmann DL (2011) StalAge: An algorithm designed for construction of speleothem age models. Quat Geochronol 6: 369-382.

51. Ahmad SM, Zheng H, Raza W, Zhou B, Lone MA, et al. (2012) Glacial to Holocene changes in the surface and deep waters of the northeast Indian Ocean. Mar Geol 331: 16-23.

52. Raza W, Ahmad SM, Lone MA, Shen CC, Sarma DS, et al. (2017) Indian summer monsoon variability in southern India during the last deglaciation: evidence from a high resolution stalagmite $\delta^{18}O$ record. Palaeogeogr Palaeocl 485: 476-485

53. Ahmad SM, Anil Babu G, Padmakumari VM, Raza W (2008) Surface and deep water changes in the northeast Indian Ocean during the last 60 ka inferred from carbon and oxygen isotopes of planktonic and benthic foraminifera. Palaeogeogr Palaeocl 262: 182-188.

54. Ólafsdóttir KB, Schulz M, Mudelsee M (2016) REDFIT-X: Cross-spectral analysis of unevenly spaced paleoclimate time series. Comput Geosci 91: 11-18.

55. Schulz M, Mudelsee M (2002) REDFIT: Estimating red-noise spectra directly from unevenly spaced paleoclimatic time series. Comput Geosci 28: 421-426.

56. Lomb NR (1976) Least-squares frequency analysis of unequally spaced data. Astrophys Space Sci 39: 447-462.

57. Scargle JD (1982) Studies in astronomical time series analysis II Statistical aspects of spectral analysis of unevenly spaced data. Astrophys J 263: 835-853.

58. Scargle JD (1989) Studies in astronomical time series analysis III Fourier transforms autocorrelation functions and cross-correlations functions of unevenly spaced data. Astrophys J 343: 874-887.

59. Spötl C, Mangini A (2002) Stalagmite from the Austrian Alps reveals Dansgaard-Oeschger events during isotope stage 3: Implications for the absolute chronology of Greenland ice cores. Earth Planet Sc Lett 203: 507-518.

60. Dreybrodt W (2008) Evolution of the isotopic composition of carbon and oxygen in a calcite precipitating $H_2OeCO_2eCaCO_3$ solution and the related isotopic composition of calcite in stalagmites. Geochim Cosmochim Ac 72: 4712e-4724.

61. Romanov D, Kaufmann G, Dreybrodt W (2008) ^{13}C profiles along growth layers of stalagmites: Comparing theoretical and experimental results. Geochim Cosmochim Ac 72: 438-448.

62. Lachniet MS (2009) Climatic and environmental controls on speleothem oxygen isotope values. Quaternary Sci Rev 28: 412-432.

63. Fleitmann D, Burns SJ, Neff U, Mudelsee M, Mangini A (2004) Palaeoclimatic interpretation of high-resolution oxygen isotope profiles derived from annually laminated speleothems from Southern Oman. Quaternary Sci Rev 23: 935-945.

64. Dorale JA, Liu Z (2009) Limitations of Hendy test criteria in judging the paleoclimatic suitability of speleothems and the need for replication. J Cave Karst Stud 71: 73-80.

65. Mühlinghaus C, Scholz D, Mangini A (2009) Modelling fractionation of stable isotopes in stalagmites. Geochim Cosmochim Ac 73: 7275-7289.

66. Zhou H, Zhao J, Qing W, Feng Y, Tang J (2011) Speleothem-derived Asian summer monsoon variations in Central China. J Quaternary Sci 26: 781-790.

67. Lone MA, Ahmad SM, Dung NC, Shen CC, Raza W (2014) Speleothem based 1000-year high resolution record of Indian monsoon variability during the last deglaciation. Palaeogeogr Palaeocl 395: 1-8.

68. Kathayat G, Cheng H, Sinha A, Spötl C, Edwards RL, et al. (2016) Indian monsoon variability on millennial-orbital timescales. Sci Rep-UK 6: 24374.

69. Kotlia BS, Singh AK, Sanwal J, Raza W, Ahmad SM, et al. (2016) Stalagmite Inferred High Resolution Climatic Changes through Pleistocene- Holocene Transition in Northwest Indian Himalaya. J Earth Sci Clim Change 7: 338.

70. Pausata FSR, Battisti DS, Nisancioglu KH, Bitz CM (2011) Chinese stalagmite $\delta^{18}O$ controlled by changes in the Indian monsoon during a simulated Heinrich event. Nat Geosci 4: 474-480.

71. Cai Y, Tan L, Cheng H, An Z, Edwards RL, et al. (2010) The variation of summer monsoon precipitation in central China since the last deglaciation. Earth Planet Sc Lett 291: 21-31.

72. Tan L, Cai Y, Cheng H, Edwards RL, Gao Y, et al. (2018) Centennial- to decadal-scale monsoon precipitation variations in the upper Hanjiang River region, China over the past 6650 years. Earth Planet Sc Lett 482: 580-590.

73. Chang X, Wang B, Yan Y, Hao Y, Zhang M (2019) Characterizing effects of monsoons and climate teleconnections on precipitation in China uses wavelet coherence and global coherence. Clim Dynam 52: 5213-5228.

74. Wang H, Chen H (2012) Climate control for southeastern China moisture and precipitation: Indian or East Asian monsoon? J Geophys Res 117: D12109.

75. Stocker TF (1994) The variable ocean. Nature 36: 221-222.

76. Tiwari RK, Yadav RR, Kaladhar Rao KPC (2012) Empirical orthogonal function spectra of extreme temperature variability decoded from tree rings of the western Himalayas. Geophys Monogr Ser 196: 169-176.

77. Ku TL, Li HC (1998) Speleothems as high-resolution paleo environment archives: Records from northeastern China. P Indian As-Earth 107: 321-330.

78. Paulsen DE, Li HC, Ku TL (2003) Climate variability in central China over the last 1270 years revealed by high-resolution stalagmite records. Quaternary Sci Rev 22: 691-701.

79. Zhang HL, Yu KF, Zhao JX, Feng YX, Lin YS, et al. (2013) East Asian Summer Monsoon variations in the past 12.5 ka: High-resolution $\delta^{18}O$ record from a precisely dated aragonite stalagmite in central China. J Asian Earth Sci 73: 162-175.

80. Cai YJ, Zhang HW, Cheng H, An ZS, Edwards RL, et al. (2012) The Holocene Indian monsoon variability over the southern Tibetan Plateau and its teleconnections. Earth Planet Sc Lett 335: 135-144.

81. Stuiver M, Braziunas TF (1989) Atmospheric 14C and century-scale solar oscillations. Nature 338: 405-408